九州大学大学院総合理工学府報告
第 41 巻 第 2 号 30-37 頁 令和 2 年 2 月

Engineering Sciences Reports, Kyushu University
Vol. 41, No. 2, pp. 30-37, FEB, 2020

Synthesis of Au@Ni Core–shell Nanoparticles Using $NaBH_4$ or L-ascorbic Acid as a Reducing agent

Masaharu TSUJI[*1,2†] Kento FUKUTOMI[*3] Masashi HATTORI[*1]
Keiko UTO[*1] Jun-Ichiro HAYASHI[*1,2] and Takeshi TSUJI[*4]
[†]E-mail of corresponding author: tsuji@cm.kyushu-u.ac.jp

(Received January 23, 2020, accepted January 30, 2020)

Au@Ni core–shell nanoparticles were synthesized using Au nanorods (NRs) as seeds. The resultant crystal structures were characterized using transmission electron microscopic (TEM) and TEM-energy dispersed X-ray spectroscopic (EDS) measurements, and ultraviolet (UV)-visible (Vis)-near infrared (NIR) extinction spectra. Ni shells were grown over AuNRs seeds by reducing $Ni(NO_3)_2{\cdot}6H_2O$ using $NaBH_4$ or L-ascorbic acid. When $NaBH_4$ was used, AuNR@Ni nanoparticles having egg-like Ni shells and small spherical Ni aggregate shells were produced. On the other hand, AuNR@Ni nanoparticles having irregular shaped Ni shells were produced by using L-ascorbic acid. The nonoccurrence of layered epitaxial growth for AuNR@Ni particles was attributed to the presence of unstable high-index {250} or {5 12 0} facets in AuNRs and a large lattice mismatch between Au and Ni (13.6%). When Ni shells were formed over AuNRs, characteristic surface plasmon resonance bands of AuNR cores became either weak or disappeared, and a long tail band originating from Ni-shell component was observed in the 350–1150 nm region.

Key words: *Au@Ni core-shell nanorods, Reducing agent, $NaBH_4$, Ascorbic acid, TEM, TEM-EDS, Surface plasmon resonance band*

1. Introduction

Core-shell nanoparticles which are constructed from more than one metallic phase have been received especial interest because of their higher catalytic, optical, electric, or magnetic properties than those of individual monometallic particles.[1-14] Since above properties strongly depend on size, shape, and composition of nanoparticles, their controlled syntheses of core-shell nanoparticles are required. An ideal method to prepare size, shape, and composition controlled core-shell nanoparticles is epitaxial growth of core-shell particles. Using a strong shape correlation between cores and shells, shape controlled epitaxial growth of shells over various shapes of core metals is possible.[15-19] Compared with extensive studies on shape controlled syntheses of core-shell nanoparticles of novel metals like Au and Ag, little work has been conducted for the syntheses of nanoparticles involving transition metals such as Cu and Ni. Although it has generally been believed that the epitaxial growth of a metal shell onto a different metal can only take place when the lattice mismatch between core and shell metals is below 5%,[17] we have demonstrated that Cu can be epitaxially grown on various shapes of Au seeds in spite of their large lattice mismatch (11.4% for Au–Cu).[20,21] As Au seeds, we used not only octahedral, triangular and hexagonal plate-like, decahedral, and icosahedral Au core seeds having low-index {100} and {111} facets but also NRs having higher-index {250} or {5 12 0} facets. The growth rates of Cu shells on sharp corners of Au cores were slower than those on flat {111} facets and single twin facets.

We have also studied epitaxial growth of Au@Ni nanocrystals with higher lattice mismatch (13.6% for Au–Ni) using octahedral, triangular and hexagonal plate-like, decahedral, and icosahedral nanocrystals as Au seeds.[22] We demonstrated that epitaxial layered growth of Ni shells over polygonal Au cores can also occur despite a larger lattice

*1 Institute for Materials Chemistry and Engineering, and Research and Education Center of Green Technology
*2 Department of Applied Science for Electronics and Materials
*3 Department of Applied Science for Electronics and Materials, Graduate Student
*4 Department of Materials Science, Shimane University

mismatch of Au–Ni. Favorable facet of Ni shells was {111}, which was the same as the major facet of Au core seeds, as in the case of Au@Cu.[20] The selected area electron diffraction (SAED) patterns indicated that single crystals of Ni layers formed parallel to those of Au seeds. For Au@Ni crystals, Ni shells were grown not only on flat {111} planes but also sharp corners of Au cores with the same thickness.

On the basis of our previous studies, there is an exceptional case that epitaxial growth can occur on sharp corners even though the lattice mismatch is as large as 13.6%. The UV- Vis-NIR spectra of Au@Ni nanoparticles gave a similar spectrum to that of Ni particle, indicating that Au@Ni particles have similar optical properties to those of Ni shells.

In this study, syntheses of AuNR@Ni nanoparticles are investigated. The purpose of this study is whether epitaxial growth occurs for AuNR@Ni nanoparticles. The effects of experimental parameters, such as a reducing agent, $NaBH_4$ or L-ascorbic acid, and their concentrations, are examined for the crystal growth of Ni shells over AuNRs.

2. Experimental

2.1 Materials

For use in this study, AuNRs involving 1.5 mM Au atoms and cetyltrimethylammonium bromide (CTAB) in an aqueous solution, were supplied by Dai-Nippon Toryo Co. Ltd. They were prepared using a photochemical method,[23] The aspect ratio of the AuNRs was about 5 (50 nm length, 10 nm diameter; W4 type). $NaBH_4$ (>97.0%), $Ni(NO_3)_2{\cdot}6H_2O$ (>98.0%), sodium citrate ($Na_3C_6H_5O_7{\cdot}2H_2O$), CTAB (>99.0%), L-ascorbic acid (>99.6%), distilled H_2O (HPLC level), and C_2H_5OH (>99.5%) were purchased from Kishida Chemical Industry Ltd. Polyethylene glycol (PEG) with an average molecular weight of 600 was obtained from Tokyo Chemical Ind. A high purity Ar gas (>99.999%) was obtained from Japan Fine Products. All reagents were used without further purification.

2.2 Synthesis of AuNR@Ni nanoparticles using $NaBH_4$ as a reducing agent

Fig. 1 shows a schematic diagram of experimental apparatus used for the synthesis of AuNR@Ni nanoparticles. The apparatus consists of a three-necked glass frasco, mechanical stirrer, a syringe pump, an optical fiber thermometer (not shown in Fig. 1), and an

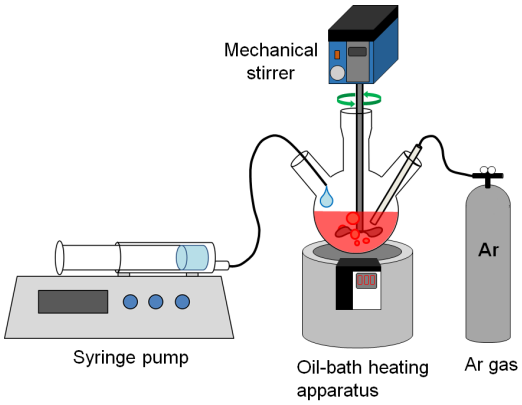

Fig. 1. Oil-bath heating apparatus used for the synthesis of Au@Ni nanoparticles.

Ar gas cylinder. 2 ml of Au seed aqueous solution was mixed with 5 ml of 15 mM $Ni(NO_3)_2{\cdot}6H_2O$ aqueous solution, 3 ml of 5 mM $Na_3C_6H_5O_7{\cdot}2H_2O$ aqueous solution, 5 ml of 36 mM CTAB aqueous solution. After bubbling Ar gas at a flow rate of 10 sccm for 30 min to remove O_2 dissolved in a reagent solution, 5 ml of $NaBH_4$ aqueous solution was injected using the syringe pump at an injection rate of 0.3 ml/min for 30 min. Ar bubbling was continued during reaction to suppress oxidation. Three different concentrations of $NaBH_4$ solution, 60, 6, or 3 mM, were examined.

2.3 Synthesis of AuNR@Ni nanoparticles using L-ascorbic acid as a reducing agent

2 ml of Au seed aqueous solution was mixed with 5 ml of 15 mM $Ni(NO_3)_2{\cdot}6H_2O$ aqueous solution, 3 ml of 5 mM NaOH aqueous solution, and 5 ml of 3 mM PEG aqueous solution under Ar gas bubbling. It was heated at 60 °C. Then, 5 ml of L-ascorbic acid was injected using the syringe pump at a rate of 0.0417 ml/min for about 2 h. The concentration of L-ascorbic acid was 30 mM or 3 mM.

2.4 Characterization of product particles

AuNR@Ni particles were obtained from C_2H_5OH solution by centrifuging the colloidal solution at 15,000 rpm for 30 min three times for TEM (JEM-2100XS; JEOL) observations. Extinction spectra of the product solutions were measured in the UV-Vis-NIR region using a spectrometer (UV-3600; Shimadzu Corp.).

3. Results and discussion

3.1 AuNR@Ni nanoparticles prepared using $NaBH_4$

Figs. 2a and 3a-3f show TEM and TEM-EDS data of AuNR@Ni nanoparticles prepared at an $NaBH_4$ concentration of 60 mM and a line analysis data along a line shown in Fig. 3d. Because the electron density of Ni is lower than that of Au, Ni and Au components are observed by light contrast and dark one in TEM images, respectively (Figs. 2a and 3a). Results show that some AuNR@Ni nanoparticles having low-density Ni shells are formed, as shown in TEM-EDS images (Figs. 3b-3d). The Au : Ni atomic ratio of AuNR@Ni particle in Fig. 3 was estimated to be 2.5 : 97.5% from EDS data. At a high $NaBH_4$ concentration, the reduction rate of Ni^{2+} is too fast so that Ni atoms concentration becomes higher than its supersaturation. Under such a condition, Ni particles are formed not only around AuNRs but also outside AuNRs. Therefore, the Ni component is distributed in a wide range, so that the high atomic ratio of Ni was obtained.

Figs. 2b, 2c, 4a-4f, and 5a-5f show corresponding TEM and TEM-EDS data at 6 and 3 mM. At 6 mM, AuNR@Ni particles, which have a larger difference in dark (AuNR core) and light (Ni shell) contrast in TEM images than that in 60 mM, are obtained (cf. Figs. 2a and 2b). This suggests that the density of Ni shells on AuNRs at 6 mM is higher than that at

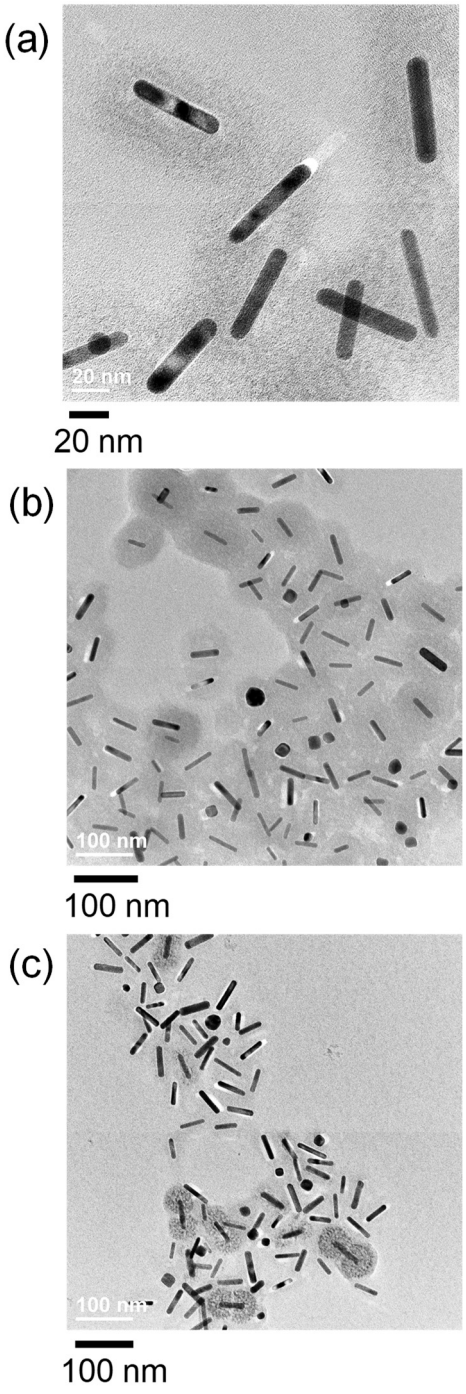

Fig. 2. TEM image of AuNR@Ni nanoparticles prepared using $NaBH_4$ at (a) 60 mM, (b) 6 mM, and (c) 3 mM.

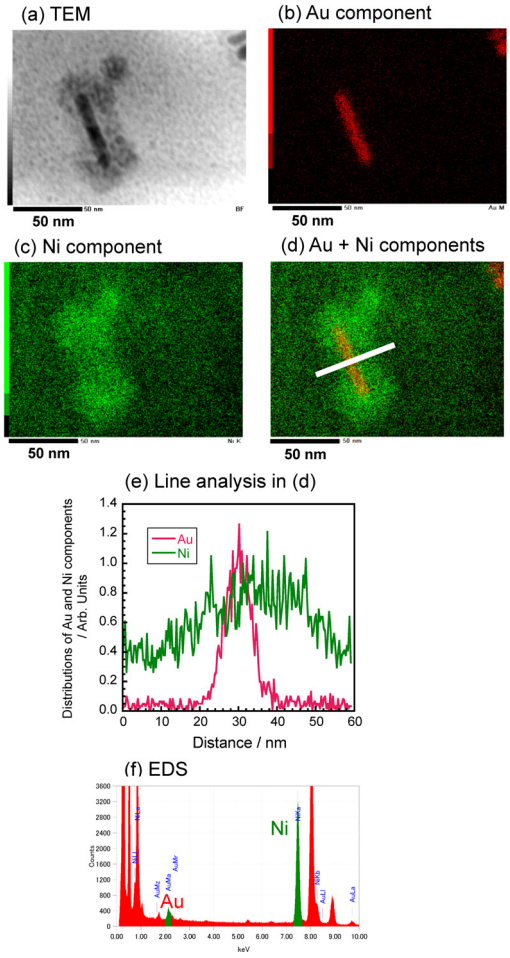

Fig. 3. TEM and TEM-EDS data of AuNR@Ni nanoparticles prepared using $NaBH_4$ at 60 mM.

60 mM. The average thickness of Ni shells was about 30–60 nm. Little Ni particles without AuNR cores were observed, indicating that 6 mM is a better concentration than 60 mM for the synthesis of AuNR@Ni particles with higher density egg-like Ni shells as a major product. In addition to AuNR@Ni particles having uniform egg-like Ni shells, some AuNR@Ni nanoparticles, which consist of uniform aggregation of small Ni particles, are observed as a minor product at 6 mM (e.g. Figs. 4a-4d). The average diameter of each spherical Ni nanoparticle was about 2 nm and the thickness of Ni aggregation shell was 30–50 nm. The Au : Ni atomic ratio of this AuNR@Ni particles in Figs. 4a-4f was estimated to be 13 : 87% from EDS data.

At 3 mM, products consist of two components, which are also observed at 6 mM. One is AuNR@Ni particles having aggregates of small Ni nanoparticles. Ni aggregate shells are composed of two parts (Figs. 5a-5d); dense Ni aggregate shells over AuNRs cores are covered by low-density Ni aggregates. The thicknesses of high- and low-density Ni aggregates were about 30–50 and 30–50 nm, respectively. Another component consists of AuNR@Ni particles having low-density Ni shells without Ni aggregates. This component was a major product at 6 mM. The density of Ni shells at 3 mM was lower than that obtained at 6 mM (cf. Figs. 2b and 2c). The Au : Ni atomic ratio of AuNR@Ni particle shown in Figs. 5a-5f was estimated to be 12 : 88% from EDS data.

On the basis of above facts, AuNR@Ni particles with egg-like Ni shells and Ni aggregates are formed using $NaBH_4$ at low concentrations of 6 and 3 mM. No layered epitaxial growth of Ni shells having well-defined facets (e.g. rectangular shape) was observed.

Fig. 6 shows UV-Vis-NIR extinction spectra of AuNRs and AuNR@Ni nanoparticles. The extinction spectrum of Au NRs gives a

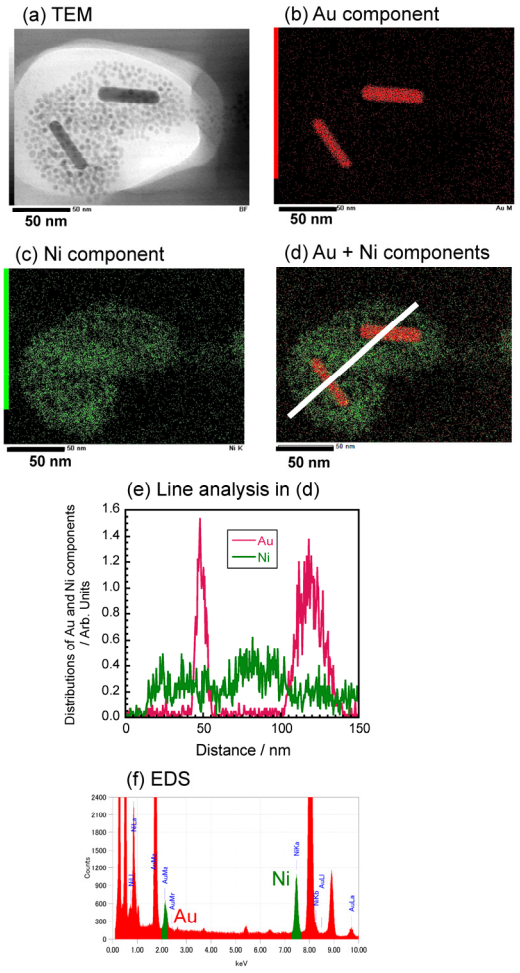

Fig. 4. TEM and TEM-EDS data of AuNR@Ni nanoparticles prepared using $NaBH_4$ at 6 mM.

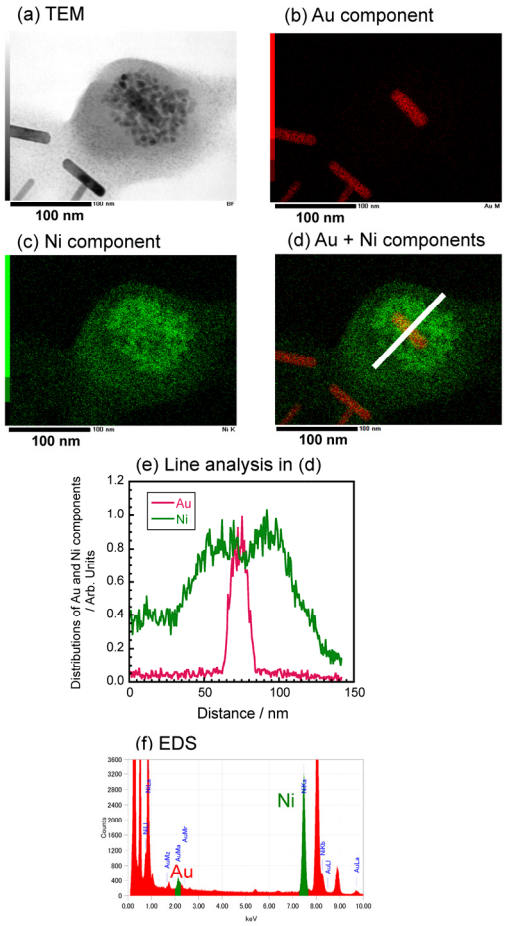

Fig. 5. TEM and TEM-EDS data of AuNR@Ni nanoparticles prepared using $NaBH_4$ at 3 mM.

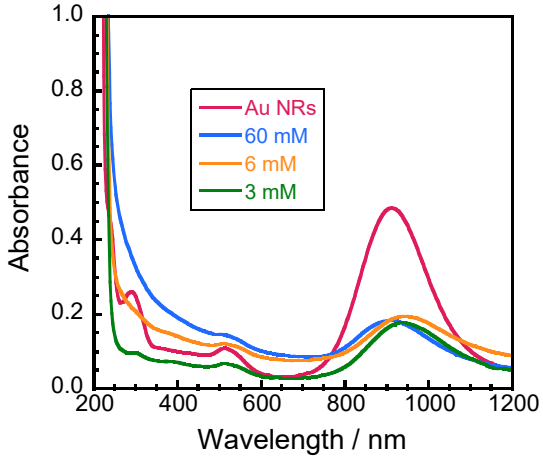

Fig. 6. UV-VIS-NIR spectra of AuNRs and AuNR@Ni particles prepared using $NaBH_4$.

longitudinal surface plasma resonance (LSPR) band at about 910 nm with a full width at half maximum (FWHM) of about 200 nm and a weak transverse SPR band at about 510 nm. When Ni shells are formed at $NaBH_4$ concentration of 60, 6, and 3 mM, the 910 nm band becomes weak and slight peak shifts to shorter wavelength (about 10 nm) at 60 mM and to longer wavelength (about 30 nm) at 6 and 3 mM are observed. In addition to peaks at 900–940 nm and 510 nm region originating from Au core components, weak tail bands are observed in the 300–750 nm region. These weak tail bands are attributable to the Ni components of AuNR@Ni and Ni particles in each condition.[22] The relative intensity of the tail bands to that of the 910 nm AuNR main bands becomes weak with decreasing the $NaBH_4$ concentration. This shows that the relative amount of Ni component in the products decreases with decreasing the $NaBH_4$ concentration.

3.2 AuNR@Ni nanoparticles prepared using L-ascorbic acid

Figs. 7a and 8a-8f show TEM and TEM-EDS data of AuNR@Ni nanoparticles prepared at a L-ascorbic acid concentration of 30 mM and a line analysis data along a line shown in Fig. 8d. Results show that thin irregular shapes of Ni shells are overgrown on AuNRs and their distributions are slightly high around the AuNRs. Ni shells over AuNRs are not flat shape, indicating that layered epitaxial Ni shell growth does not occur in this condition. No Ni aggregate shells were observed using L-ascorbic acid. The Au : Ni atomic ratio of this AuNR@Ni particle in Figs. 8a-8f was estimated

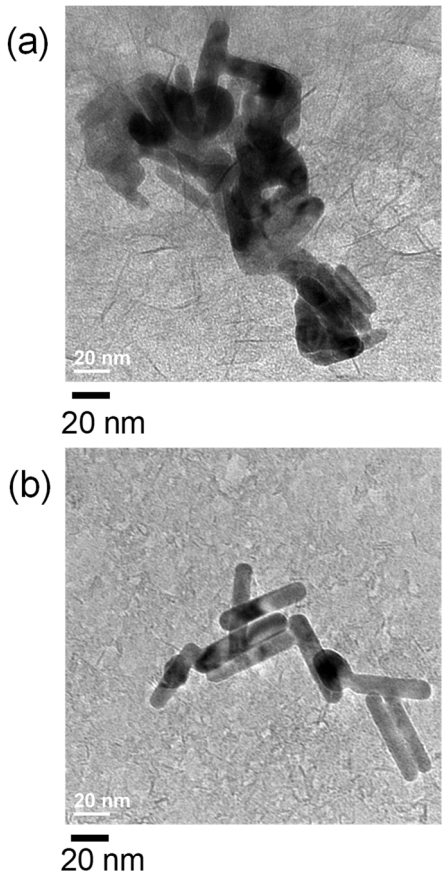

Fig. 7. TEM image of AuNR@Ni nanoparticles prepared using L-ascorbic acid at (a) 30 mM, and (b) 3 mM.

to 75 : 25% from EDS data.

Figs. 7b and 9a-9f show corresponding data of AuNR@Ni at a lower L-ascorbic acid concentration of 3 mM. Although layered Ni shells are not formed, the formation of low density of Ni shells are observed around AuNRs. The Au : Ni atomic ratio of AuNR@Ni particles in Figs. 9a-9f was estimated to be 75 : 25% from EDS data. Ni component was distributed in a wider space range than that at 30 mM. Therefore, a similar Au : Ni atomic ratio was obtained even though the density of Ni shells around AuNRs was low.

Fig. 10 show UV-Vis-NIR extinction spectra of AuNRs and AuNR@Ni nanoparticles obtained using L-ascorbic acid at 30 and 3 mM. At 30 mM, a long tail band of Ni component is observed in the 350–1150 nm region and no Au peak at 910 nm is observed. This suggests that AuNRs are fully covered by Ni component in this condition. At a lower concentration of 3 mM a weak AuNR component and a weak tail band of Ni component appear. These spectral features are consistent with the observations

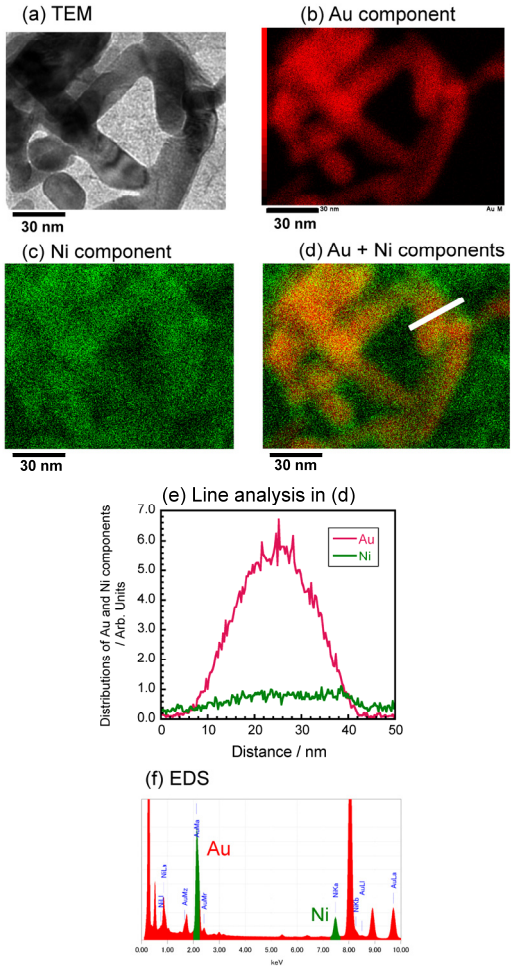

Fig. 8. TEM image of AuNR@Ni nanoparticles prepared using L-ascorbic acid at 30 mM.

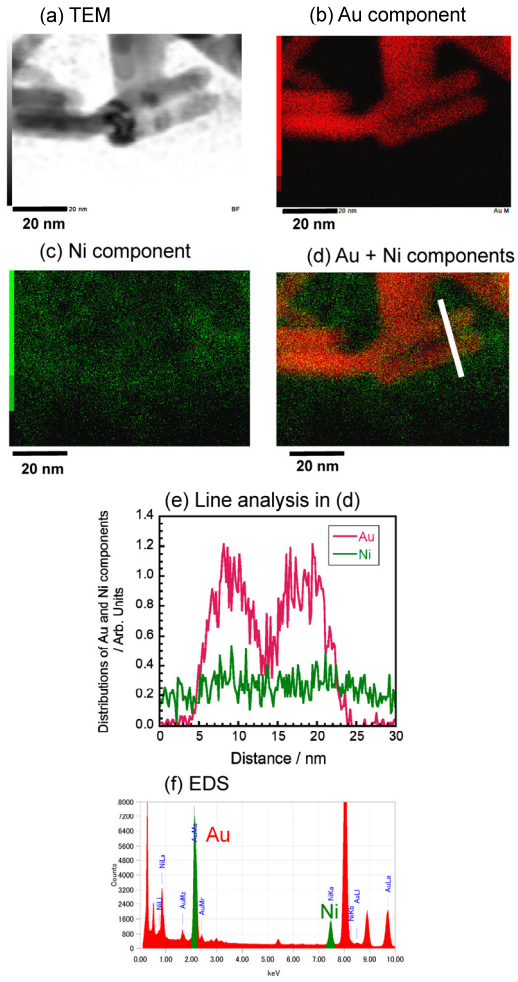

Fig. 9. TEM image of AuNR@Ni nanoparticles prepared using L-ascorbic acid at 3 mM.

from TEM and TEM-EDS images, in which AuNRs at 3 mM are covered by lower density Ni shells than those at 30 mM. On the basis of SPR data, more dense Ni shells, which suppress the optical property of AuNR core component, are formed by using L-ascorbic acid. Thus, the optical property of AuNR@Ni particles can be controlled by changing the L-ascorbic acid concentration.

3.3 Growth mechanism of AuNR@Ni nanoparticles

We have previously found rectangular AuNR@Pd particles having {100} facets are dominantly formed when Pd shells were overgrown on AuNRs having {250}, {5 12 0}, {100}, and {110} facets (Fig. 11).[21,25] If similar epitaxial growth occurs, rectangular shaped AuNR@Ni particles will be formed (Fig. 11a). However, such rectangular shapes of AuNR@Ni

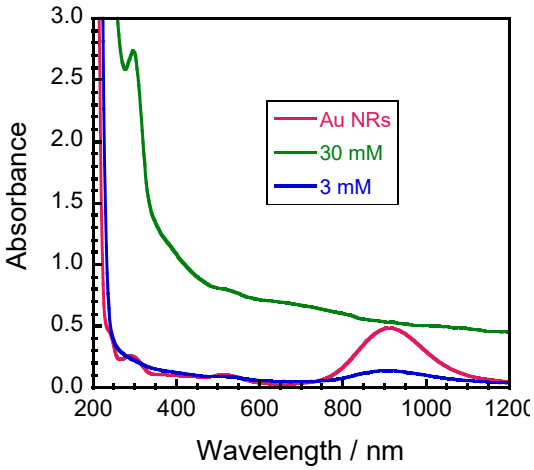

Fig. 10. UV-VIS-NIR spectra of AuNRs and AuNR@Ni particles prepared using L-ascorbic acid.

particles were not obtained in this work. When $NaBH_4$ was used as a strong reducing agent, AuNR@Ni nanoparticles having egg-like Ni shells (Fig. 11b) and small spherical Ni aggregates (Fig. 11c) were produced. On the other hand, AuNR@Ni nanoparticles having irregular shaped Ni shells were produced by using L-ascorbic acid as a weak reducing agent (Fig. 11d). In our previous study on Au@Ni,[22] Ni shells were epitaxially grown over octahedral, triangular and hexagonal plate-like, decahedral, and icosahedral Au core seeds, even though lattice mismatch between Au and Ni is as large as 13.6%. However, such epitaxial growth of Ni shells was not observed for AuNR core seeds in this study. A major reason for non-observation of epitaxial growth of Ni shells will be the existence of high-index {250} or {5 12 0} facets in AuNRs. Epitaxial layered growth over such high-index facets having high surface energies is more difficult than that over stable low-index {100} and {111} facets having low surface energies. This will be a major reason why the layered growth of Ni shells was not observed for AuNRs. Although epitaxial layered growth was observed for AuNR@Cu,[21] it was not found for AuNR@Ni using the same AuNRs with high-index {250} or {5 12 0} facets in this study. The lattice mismatch between Au and Ni (13.6%) is larger than that between Au and Cu (11.4%). The large lattice mismatch between Au core and Ni shell atoms will be another reason for non-observation of epitaxial growth of AuNR@Ni particles.

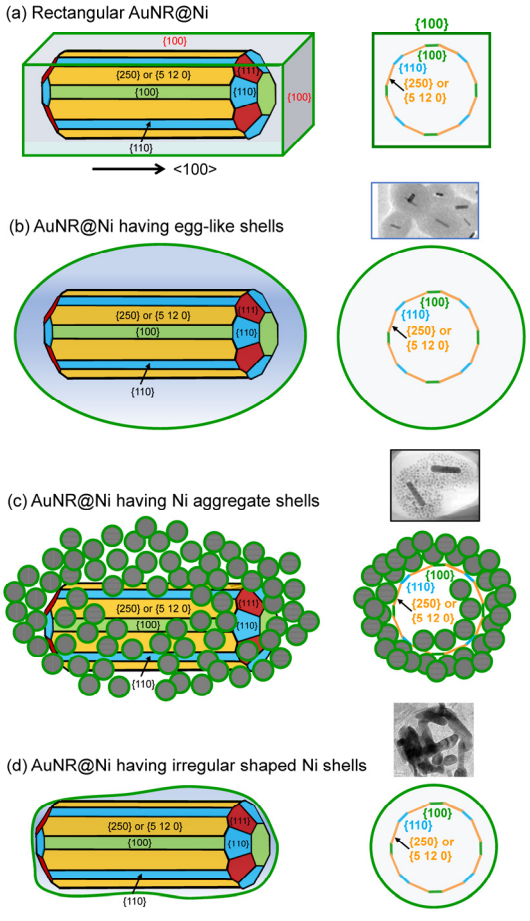

Fig. 11. Four types of AuNR@Ni particles.

4. Summary and Conclusion

AuNR@Ni core-shell nanorods were prepared by reducing $Ni(NO_3)_2{\cdot}6H_2O$ using $NaBH_4$ or L-ascorbic acid as strong or weak reducing agent, respectively. When $NaBH_4$ was used, egg-like Ni shells and Ni aggregate shells were formed. On the other hand, AuNR@Ni particles having irregular shapes of Ni shells were produced by using L-ascorbic acid. Although Ni shells were epitaxially grown over octahedral, triangular and hexagonal plate-like, decahedral, and icosahedral Au core seeds having low-index {100} and {111} facets in our previous study,[22] no epitaxial growth of rectangular AuNR@Ni particles was observed using AuNR seeds in this study. The lack of epitaxial growth using AuNRs was explained by the presence of high-index {250} or {5 12 0} facets in AuNRs and large lattice mismatch between Au core and Ni shell atoms (13.6%). In this work, AuNR@Ni particles having egg-like Ni shells, Ni aggregate shells, and/or irregular shaped Ni shells were obtained, although their yields depended on the reducing agent and its concentration. These new shaped AuNR@Ni may give unique catalytic and magnetic properties.

Acknowledgments

We thank Dai-Nippon Toryo Co. Ltd. for suppling us AuNRs used in this study. This work was supported by JSPS KAKENHI Grant number 25286003.

References

1) L. M. Liz-Marzán, M. Giersig, and P. Mulvaney, *Langmuir*, 12, 4329 (1996).
2) C. J. Zhong and M. M. Maye, *Adv. Mater.*, 13, 1507 (2001).
3) C. Xue, J. E. Millstone, S. Li, and C. A. Mirkin, *Angew. Chem., Int. Ed.*, 46, 8436 (2007).
4) Y. Yang, J. Shi, G. Kawamura, and M. Nogami, *Scripta Materialia*, 58, 862 (2008).
5) K. J. Majo, C. De, and S. O. Obare, *Plasmonics*, 2009, 4, 61 (2009).

6) Y. Xia, Y. Xiong, B. Lim, and S. E. Skrabalak, *Angew. Chem. Int. Ed.*, 48, 60 (2009).
7) B. P. Khanal and E. R. Zubarev, *Angew. Chem. Int. Ed.*, 48, 6888 (2009).
8) R. Hao, R. Xing, Z. Xu, Y. Hou, S. Gao, and S. Sun, *Adv. Mater.*, 22, 2729 (2010).
9) M. Baghbanzadeh, L. Carbone, P. D. Cozzoli, and C. O. Kappe, *Angew. Chem. Int. Ed.*, 50, 11312 (2011).
10) M. B. Cortie and A. M. McDonagh, *Chem. Rev.*, 111, 3713 (2011).
11) R. G. Chaudhuri and S. Paria, *Chem. Rev.*, 112, 2373 (2012).
12) X. Liu, Y. Sun, C. Feng, C. Jin, and F. Xiao, *J. Power Sources*, 245, 256 (2014).
13) M. Tsuji, N. Miyamae, S. Lim, K. Kimura, X. Zhang, S. Hikino, and M. Nishio, *Cryst. Growth Des.*, 6, 1801 (2006); M. Tsuji, R. Matsuo, P. Jiang, N. Miyamae, D. Ueyama, M. Nishio, S. Hikino, H. Kumagae, K. S. N. Kamarudin, and X.-L. Tang, *Cryst. Growth Des.*, 8, 2528 (2008); M. Tsuji, N. Nakamura, M. Ogino, K. Ikedo, and M. Matsunaga, *CrystEngComm*, 14, 7639 (2012).
14) M. B. Gawande, A. Goswami, T. Asefa, H. Guo, A. V. Biradar, D.-L. Peng, R. Zboril and R. S. Varma, *Chem. Soc. Rev.,* 44, 7540 (2015).
15) Y. Xiang, X. Wu, D. Liu, X. Jiang, W. Chu, X. Li, Y. Ma, W. Zhou, and S. Xie, *Nano Lett.*, 6, 2290 (2006).
16) S. E. Habas, H. Lee, V. Radmilovic, G. A. Somorjai, and P. Yang, *Nature Mater.*, 6, 692 (2007).
17) F.-R. Fan, D.-Y. Liu, Y.-F. Wu, S. Duan, Z.-X. Xie, Z.-Y. Jiang, and Z.-Q. Tain, *J. Am. Chem. Soc.*, 130, 6949 (2008).
18) F. Wang, L. D. Sun, W. Feng, H. Chen, M. H. Yeung, J. Wang, and C. H. Yan, *Small*, 6, 2566 (2010).
19) W. Annan, P. Qing, and L. Yadong, *Chem. Mater.*, 23, 3217 (2011).
20) M. Tsuji, D. Yamaguchi, M. Matsunaga, and M. J. Alam, *Cryst. Growth Des.*, 10, 5129 (2010).
21) Y. Yoshida, K. Uto, M. Hattori, and M. Tsuji, *CrystEngComm*, 16, 5672 (2014).
22) M. Tsuji, D. Yamaguchi, M. Matsunaga, and K. Ikedo, *Cryst. Growth Des.*, 11, 1995 (2011).
23) Y. Niidome, K. Nishioka, H. Kawasaki, and S. Yamada, *Chem. Commun.*, 2376 (2003).
24) M. Tsuji, K. Ikedo, K. Uto, M. Matsunaga, Y. Yoshida, K. Takemura, and Y. Niidome, *CrystEngComm*, 15, 6553 (2013).
25) M. Tsuji, K. Takemura, C. Shiraishi, K. Ikedo, K. Uto, A. Yajima, M. Hattori, Y. Nakashima, K. Fukutomi, K. Tsuruda, T. Daio, T. Tsuji, and S. Hata, *J. Phys. Chem. C*, 119, 10811 (2015).